PHYSICAL REVIEW B VOLUME 27, NUMBER 6 15 MARCH 1983

Exciton and magnon-sideband absorption in the pyroelectric antiferromagnet $BaMnF_4$

Taiju Tsuboi*
Physics Department, Kyoto Sangyo University, Kamigamo, Kyoto 603, Japan

W. Kleemann†
Fachbereich 6 (Physik), Universität—Gesamthochschule Paderborn, D-4790 Paderborn, Federal Republic of Germany
(Received 14 October 1982)

Polarized absorption and luminescence spectra of the pyroelectric antiferromagnet $BaMnF_4$ are measured in the temperature range 4.5—300 K. Single-exciton bands associated with Mn^{2+} ions, as well as double-exciton bands, are observed. The temperature dependence of the integrated intensities of both bands suggests that exchange-assisted electric dipole transitions are dominantly involved. It is shown for the single-exciton band corresponding to the ${}^6A_{1g}\rightarrow{}^4T_{2g}$ (II) transition that the fine structure observed consists of an *electric-dipole-allowed* pure exciton band and hot- and cold-magnon sidebands. A three-magnon hot band is found for the first time. The analyses of optical anisotropy in the pure exciton band indicate that the Mn^{2+} ion is displaced from a nearly cubic position along the a-axis direction by the pyroelectric moment due to Ba^{2+} ions. The observed temperature dependences of the peak positions and of the half-widths of the magnon sidebands are consistent with the appearance of three-dimensional spin ordering below T_N, although $BaMnF_4$ is a predominantly two-dimensional antiferromagnet. An emission band observed at 600 nm is discussed involving short-range exciton transfer from Mn^{2+} to impurity-perturbed Mn^{2+} ions.

I. INTRODUCTION

$BaMnF_4$ has a layered orthorhombic crystal structure with the crystal symmetry of $A2_1am$ (C_{2v}^{12}) at room temperature ($a=5.984$ Å, $b=15.098$ Å, $c=4.216$ Å.[1] The structure consists of disordered MnF_6 octahedra sharing corners to form puckered sheets perpendicular to the b axis; the sheets are linked by Ba^{2+} ions. The Mn—F—Mn—F chains are nearly linear along the c axis, whereas the chains connecting two shared F^- ions zig zag along the a axis. The magnetic study shows that $BaMnF_4$ is antiferromagnetic ($T_N=27$ K), with two-dimensional ordering in the temperature range between about 70 K and T_N, whereas three-dimensional ordering occurs below T_N.[2,3] On the other hand, from the dielectric study, $BaMnF_4$ is also classified as a member of pyroelectric materials.[3] A considerable amount of study has been done on the magnetic and dielectric properties of $BaMnF_4$, especially related to structural and magnetic phase transitions.[3–5] On the other hand, much less is known about the optical properties. So far, Régis *et al.*[6] and St.-Grégoire[7] studied the linear dichroism of the optical absorption band observed at 395—400 nm in order to investigate the structural phase transition appearing at $T_c=250$ K. Goldberg *et al.* observed the red luminescence of $BaMnF_4$,[8] and Moncorgé and Jacquier found the exciton and exciton-magnon fine structure in the excitation and emission spectra using laser excitation.[9]

The optical properties of other antiferromagnetic Mn^{2+} compounds such as MnF_2 have been intensively studied, especially on the magnon sidebands of single-exciton bands associated with the $d^5\rightarrow d^5$ transition in Mn^{2+} ions.[10,11] The magnon sidebands appearing on the tails of exciton bands have been attributed to spin-exchange-induced electric dipole transitions, whereas the exciton band is due to a magnetic dipole transition, because the $d^5\rightarrow d^5$ transition is spin and parity forbidden in the Mn^{2+} ion with inversion symmetry.[12] An electric-dipole-allowed pure exciton band has so far been observed only in $CsMnF_3$, which has noncentrosymmetric Mn^{2+} ions.[13–15] The exciton band reflects the site symmetry of the Mn^{2+} ion more directly than does the magnon sideband, because the latter case involves the exciton-magnon and magnon-magnon interactions. Therefore the present investigation was first undertaken to examine the exciton bands in

$BaMnF_4$. In addition to the single-exciton band, double-exciton bands, which correspond to the simultaneous electronic excitation of pairs of magnetic ions, have been observed in various Mn^{2+} compounds.[16–18] There is no report on the presence of the double-exciton bands in $BaMnF_4$. Related to this point, we also investigate the absorption spectra in the high-energy region, where the double-exciton bands are expected to appear.

Three other interesting investigations are conceivable for $BaMnF_4$, which have not yet been done. The first one is optical anisotropy, which will be studied in order to investigate the local symmetry of Mn^{2+} ions, since $BaMnF_4$ has a complicated orthorhombic crystal structure. The second is the optical detection of pyroelectricity, or more precisely speaking, the optical detection of the influence of the pyroelectric moment produced by Ba^{2+} ions on the magnetic Mn^{2+} ions. Since $BaMnF_4$ is a unique material with both the pyroelectric and antiferromagnetic properties at the same time, it is expected that effects of pyroelectricity appear on the Mn^{2+} absorption bands, e.g., on the line shape. The third investigation is the optical detection of the coexistence of two- and three-dimensional antiferromagnetic spin orderings, since the presence of two kinds of dimensionality has been suggested from magnetic susceptibility measurements but has not yet been confirmed optically. In this paper, along with the above three points, we also study the polarized absorption spectra of $BaMnF_4$ in the temperature region of 4.5–300 K.

II. EXPERIMENTAL PROCEDURE

Single crystals of $BaMnF_4$ were grown by the Bridgman method in a carbon crucible from an equimolar mixture of BaF_2 and MnF_2. The samples were oriented using Laue back reflection x-ray patterns, cut parallel to the orthorhombic {100} faces and polished. Thus orthorhombic samples with (a,b), (a,c), and (b,c) planes were obtained. A (b,c)-oriented sample, which was grown at the Massachusetts Institute of Technology, MIT, was used at the initial stage of our investigations. The absorption spectra of the MIT crystal were in agreement with those of our (b,c) sample. This indicates that both samples do not contain measurable amounts of impurities. Polarized absorption spectra were recorded on a Cary 14 spectrophotometer with a Glan prism or a Polacoat polarizer. Two spectra were measured for each of the three planes, e.g., for the (a,b) plane we measured the $\vec{E}||a$ spectrum and the $\vec{E}||b$ spectrum, with the light propagating along the c axis, where $\vec{E}$ denotes the electric vector of the incident light. The luminescence spectra were measured as follows. The crystal luminescence emitted at right angles to the exciting beam was passed through a Bausch-Lomb $f=0.25$ m monochromator and detected with RCA 1P28 or a Philips 150 UVP photomultiplier. The Cary 14 monochromator was used to produce the monochromatic exciting light. A 750-W tungsten lamp was used as a light source.

III. EXPERIMENTAL RESULTS AND ANALYSES

A. Absorption bands and their energy-level assignments

Figure 1 shows the absorption spectra of $BaMnF_4$, which were measured in the (b,c) plane using unpolarized light. The whole spectrum at 295 K is quite similar to the room-temperature spectra of other Mn-F compounds, for instance, $KMnF_3$ and $RbMnF_3$.[16,19] Ten absorption bands are observed in the visible to the ultraviolet region. We call these bands A, B, C, D, E, F, α, G, β, and γ in order of increasing energy, as indicated in Fig. 1. From their temperature (T) dependence, these bands can be classified into two groups. One group consists of the α, β, and γ bands, which grow with decreasing temperature as shown in Figs. 2 and 3. According to Fujiwara *et al.*,[18] the absorption intensity of double-exciton bands in a two-equivalent-sublattice antiferromagnet has the following T dependence:

$$I_d(T)=\frac{1}{12}-\frac{\langle \vec{S}_j\cdot\vec{S}_l\rangle}{8S^2}+\frac{\langle \vec{S}_l\cdot\overleftrightarrow{Q}_j\cdot\vec{S}_l\rangle}{4S^2(2S-1)^2}\ , \tag{1}$$

where j and l are two nearest-neighbor magnetic ions and $\overleftrightarrow{Q}$ is a symmetric tensor containing bilinear spin operators. The expression (1) has been experimentally confirmed in MnF_2 and $RbMnF_3$ (Ref. 18) and in other materials.[20–22] A quite similar T dependence is observed in $BaMnF_4$, as seen in Fig. 3. Indeed, the α band gives a value $I_d(\infty)/I_d(0)=\frac{1}{3}$ experimentally, which agrees with Eq. (1) calculated for Mn^{2+} ($S=\frac{5}{2}$) in the high- and low-temperature limits. Therefore the α, β, and γ bands are attributable to double-exciton bands. On the other hand, the intensities of the other bands A–G are essentially temperature independent. They are attributable to single-exciton bands from their characteristic T dependence and their energy-level calculation as outlined below. The assignment is confirmed to be probable, since the A–G band spectrum is quite similar to the single-exciton absorption spectrum observed in $KMnF_3$, $RbMnF_3$, and MnF_2.[16,23]

Each Mn^{2+} ion in $BaMnF_4$ is surrounded by six nearest-neighbor F^- ions, forming a slightly distort-

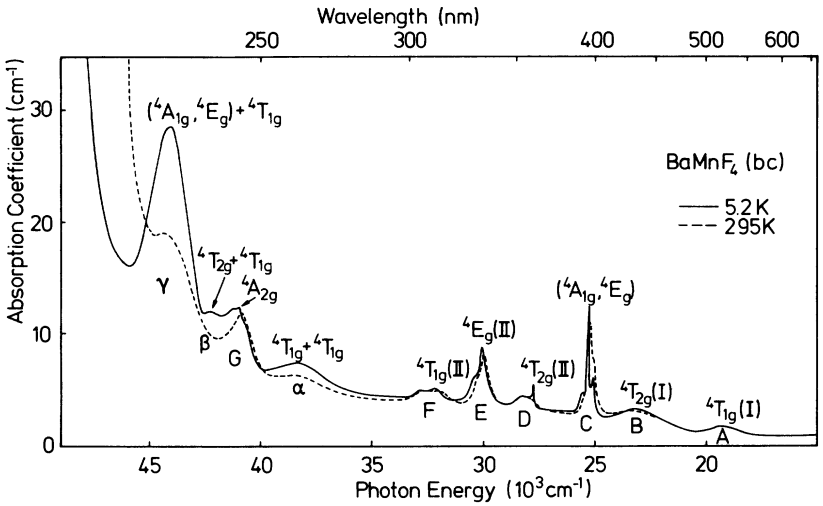

FIG. 1. Unpolarized absorption spectra of $BaMnF_4$ on the (b,c) plane at 5.2 and 295 K.

ed MnF_6 octahedron. However, it will be reasonable to use, as a starting point, the cubic-field formalism to estimate the first moments of absorption bands, since the energy-level splitting due to the low-symmetry crystal field is expected to be nearly negligible when compared with the splitting due to the cubic field. Certainly, this can be suggested from the fact that the whole absorption spectrum of $A-G$ bands is quite similar to that of $RbMnF_3$ with cubic symmetry, although the true site symmetry of Mn^{2+} in $BaMnF_4$ is only C_i. Tanabe and Sugano derived the energy matrices for the d^5 configuration ion in a cubic field,[24] which were later modified by including the covalency parameter ϵ and the Racah-Trees correction α.[23,25]

Several techniques have been proposed to evaluate the values of ϵ,α and of the Racah parameters B and C for the Mn^{2+} octahedra. For example, Stout[23] proposed to determine ϵ using the free-ion values of $B=950$ cm^{-1} and $C=3280$ cm^{-1} from the energy level of ^4E_g (II) under $\alpha=0$, Ferguson proposed to determine B and C from the energies of the $^4A_{1g}$, ^4E_g (I), and ^4E_g (II) levels under $\epsilon=0$,[16] and recently Rao and Purander[26] proposed to determine the values of B and C from the energy states ^4E_g (I) and ^4E_g (II) using the free-ion value of $\alpha=76$ cm^{-1} under $\epsilon=0$. After the evaluation of the values of B, C, ϵ, and α, the energy matrices for the $^4T_{1g}$ and $^4T_{2g}$ states are solved for various values of the octahedral–ligand-field parameter Dq, giving the so-called Tanabe-Sugano (TS) diagram. Then the Dq value is determined by comparison with the ab-

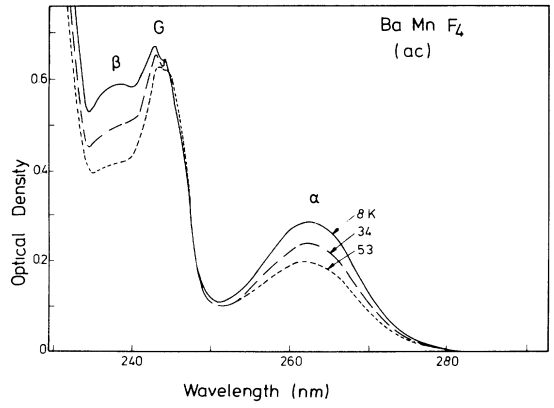

FIG. 2. Unpolarized absorption spectra in the α- and β-band region measured on the (a,c) plane at various temperatures.

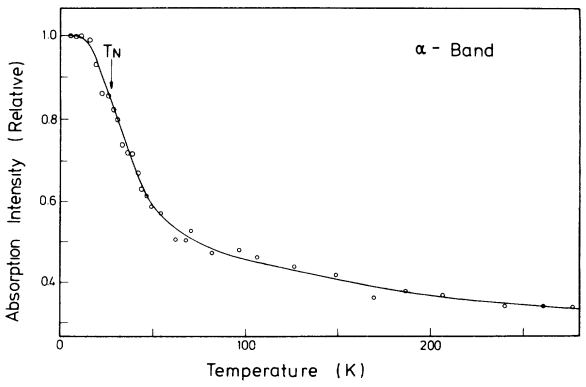

FIG. 3. Temperature dependence of the absorption intensity (band area) of the α band. The intensity is normalized at 4.5 K.

sorption spectrum. We calculated the TS diagram using these three techniques. The best one was obtained from the TS diagram calculated using Rao and Purander's technique. The best fitting parameters are found to be $B=834$ cm^{-1}, $C=3077$ cm^{-1}, $\alpha=76$ cm^{-1}, $\epsilon=0$, and $Dq=800$ cm^{-1}. The positions of the observed bands and the calculated energies relative to the $^6A_{1g}$ ground state are listed in Table I together with the band assignments. Our assignments agree with those made by St.-Grégoire[7] except for the G band. St.-Grégoire assigned the α and G bands to the $^4A_{2g}$ and $^4T_{1g}$ (III) states, respectively, but the α band must be assigned to a double-exciton band as discussed above. Our assignment is quite consistent with the case of $RbMnF_3$, as was expected from the similarity of the spectra.[16] As in the case of $RbMnF_3$, two high-energy bands associated with the T_{1g} (II) and T_{2g} (III) states are not observed, both being hidden under the large α and γ bands.

Regarding the double-exciton bands, a simple method of the level assignment is to take into account their band positions, since the energy of a double-exciton band associated with the $(\Gamma_i+\Gamma_j)$ state is, in the first approximation, given by the sum of the energies of Γ_i and Γ_j states.[16] For example, the α band is located at the doubled energy of the A band. Thus the α band is believed to be produced when two Mn^{2+} ions are simultaneously excited to the same $^4T_{1g}$ (I) states. Similarly, we can assign the β and γ bands as shown in Table I. Of the three double-exciton bands observed, the α band is weaker than the others. This is consistent with the selection rule such that the pair transition should be forbidden, if the final electronic states on the two ions are identical.[27] The α band is expected to exhibit the same properties as its parent band, i.e., the A band. Indeed, the same blue shift and the same dichroism ($f_a>f_c>f_b$, where f is the oscillator strength) are observed for the α and A bands. For the γ band, which is produced when one Mn^{2+} ion of the pair is excited to the $^4T_{1g}$ (I) state and the other ion to the $^4A_{1g}$ or ^4E_g (I) state, we cannot predict which parent band, the A or C band, determines the character of the γ band. Experimentally, it is noted that the γ band does not shift on changing the temperature, similar to the C band. Hence it is suggested that the property of the γ band is determined by the C band and not by the A band.

B. Optical anisotropy of Mn^{2+} bands

The absorption spectrum of $BaMnF_4$ depends obviously on the crystal orientation, i.e., it exhibits linear dichroism. Six polarized spectra were measured: $(\vec{E}||a,\vec{L}||c)$ and $(\vec{E}||b,\vec{L}||c)$

TABLE I. Observed and calculated transition energies and observed oscillator strengths of absorption bands in $BaMnF_4$ at 4.5 K, together with their level assignments.

Single-exciton band	Assignment of excited state	Transition energy (10^3 cm^{-1}) Observed	Calculated	Oscillator strength (10^{-7}) f_a	f_b	f_c
A	$^4T_{1g}$ (I)	19.15	18.800	4.76	2.92	2.33
B	$^4T_{2g}$ (I)	23.05	23.060	1.59	1.95	2.28
C	^4E_g (I)		25.245			
		25.22		2.63	1.08	7.44
	$^4A_{1g}$		25.220			
D	$^4T_{2g}$ (II)	28.00	28.310	2.36	1.90	1.56
E	^4E_g (II)	30.05	30.050	2.42	1.27	8.36
F	$^4T_{1g}$ (II)	32.40	32.990	3.07	1.79	2.15
G	$^4A_{2g}$	40.95	40.799	~4.2	~3.4	~9.7
	$^4T_{1g}$ (III)		41.790			
	$^4T_{2g}$ (III)		44.790			
double-exciton band						
α	$^4T_{1g}$ (I)+$^4T_{1g}$ (I)	38.40	38.30[a]	7.13	5.93	5.11
β	$^4T_{1g}$ (I)+$^4T_{2g}$ (I)	42.25	42.20[a]			0.28
γ	$^4T_{1g}$ (I)+(^4E_g (I),$^4A_{1g}$)	44.05	44.37[a]	85.8	61.5	32.7

[a]Estimated using the observed single-exciton energies.

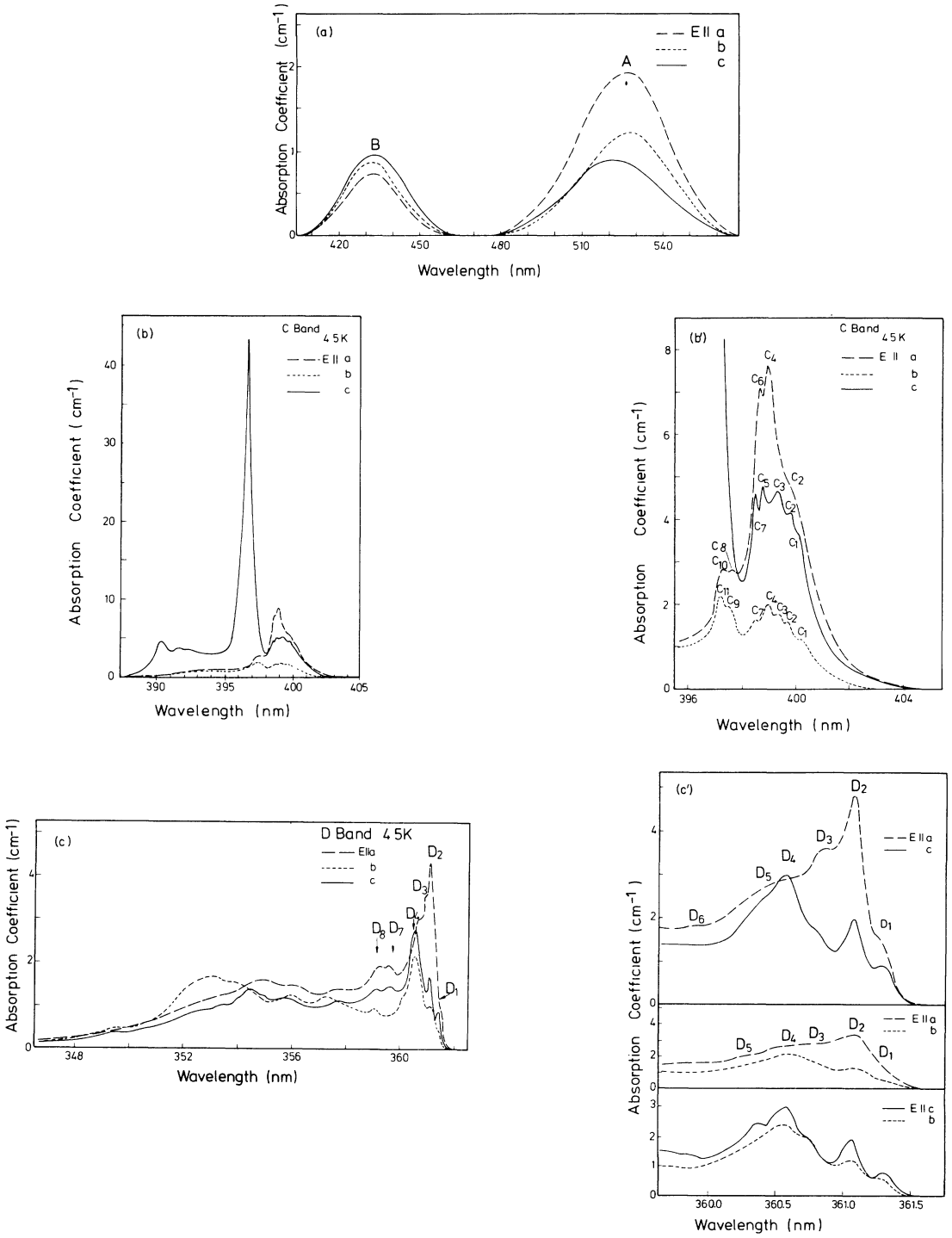

FIG. 4. $\vec{E}||a$, $\vec{E}||b$, and $\vec{E}||c$ spectra at 4.5 K of (a) the *A* and *B* bands, (b) *C* band, (b') fine structure at the low-energy side of the *C* band, (c) *D* band, (c') fine structure at the low- energy side of the *D* band measured on the (*a*,*c*) plane (upper figure), (*a*,*b*) plane (middle), and (*b*,*c*) plane (bottom), (d) *E* band, (e) *F* band, and (f) α, β, γ, and *G* bands on the (*a*,*c*), (*a*,*b*), and (*b*,*c*) planes, respectively.

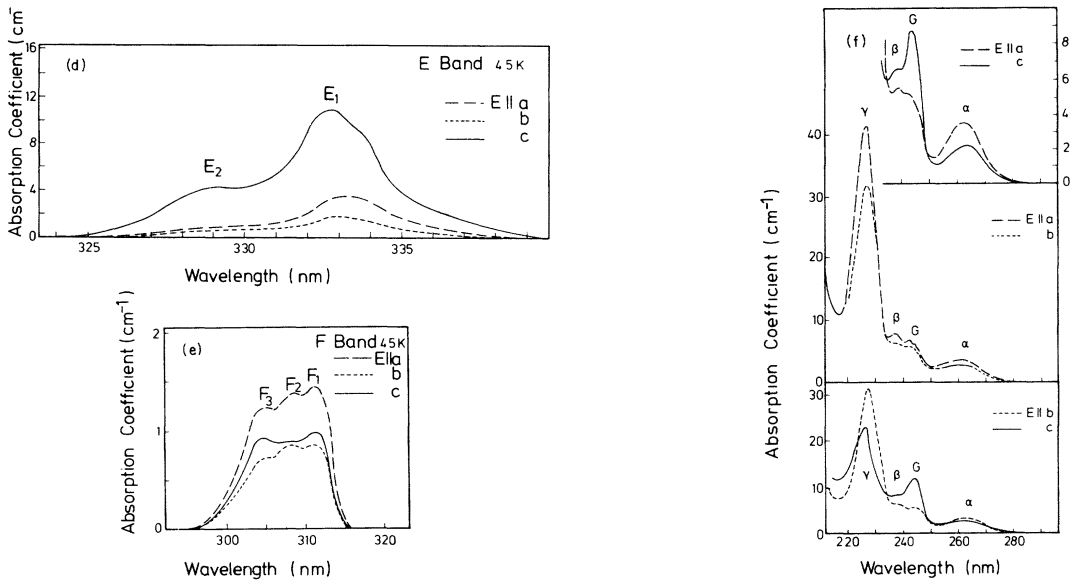

FIG. 4. (*Continued.*)

spectra for the (a,b) plane, $(\vec{E}||b,\vec{L}||a)$ and $(\vec{E}||c,\vec{L}||a)$ spectra for the (b,c) plane, and $(\vec{E}||a,\vec{L}||b)$ and $(\vec{E}||c,\vec{L}||b)$ spectra for the (a,c) plane, where $\vec{L}$ denotes the direction of incident light. When the spectra (line shape, position, and intensity) of all the bands are compared among the six polarized spectra, it is concluded that the spectra taken at the same $\vec{E}$ direction [e.g., $(\vec{E}||a,\vec{L}||b)$ and $(\vec{E}||a,\vec{L}||c)$ spectra] are completely identical with each other as seen in Figs. 4(c') and 4(f). Evidently, the structure of the spectrum is affected only by the change of the $\vec{E}$ direction, whereas the $\vec{L}$ direction has no appreciable influence. This indicates that all the bands, including their fine structures, are due to electric dipole transitions. In Figs. 4(a)–4(f) the $\vec{E}||a$, $\vec{E}||b$, and $\vec{E}||c$ spectra of all the bands are shown. In order to confirm that the absorption is due to the electric dipole transition, we also measured the angular dependence of the absorption bands. One of the best candidates for the measurement is a relatively sharp absorption band peaking at 390.3 nm in the C band, since this band is observed in the $\vec{E}||c$ spectrum but not in the $\vec{E}||a$ and $\vec{E}||b$ spectra. Therefore the electric dipole moment $\vec{P}$ associated with the 390.3 nm band is believed to be parallel to the c axis. When the electric vector of incident light changes its direction from $\vec{E}||c$ to $\vec{E}||a$ in the (a,c) plane, the peak intensity is expected to be proportional to $\cos^2\theta$, where θ is the angle measured from the c axis, because the absorption intensity due to the electric dipole transition is proportional to $\langle\vec{P}\cdot\vec{E}\rangle^2$. The experimental result on the 390.3 nm band is in good agreement with the expectation. In this manner the observed absorption band is confirmed to be attributable to an electric dipole allowed transition.

The oscillator strengths f of various bands are given in Table I. In the calculation of f, we used the room-temperature refractive indices measured at 589.3 nm,[28] $n_a=1.480$, $n_b=1.505$, and $n_c=1.499$, and for the effective field correction, $E_0/E_{\text{eff}}=1$. The f values are of the same order ($f\sim10^{-7}$) as those of other Mn^{2+} compounds. The total f values of all single-exciton bands are $f_a=2.1\times10^{-6}$, $f_b=1.4\times10^{-6}$, and $f_c=3.4\times10^{-6}$ at 4.5 K. It is noted that the f value of the b-axis direction is the smallest of the three. This is interpreted as follows. The spin-exchange interactions between two Mn^{2+} ions contributes predominantly to the intensity of the single-exciton bands.[18] Thus the magnon sideband gives the most important contribution to the single-exciton absorption intensity. In $BaMnF_4$, each Mn^{2+} ion easily finds a partner in the a-and c-axis directions to form a paired Mn^{2+} center linked by a single F^- ion, giving rise to the intralayer spin-exchange interaction, whereas along the b direction more complex exchange paths are involved because of the layered structure of $BaMnF_4$. Therefore, the spin-exchange interaction of the paired Mn^{2+} ions in the b direction is weak, resulting in the weak absorption intensity.

Compared with the case of the double-exciton band (Fig. 3), quite different T dependences are obtained for the single-exciton bands. The tempera-

ture dependence of the absorption intensity is shown for the A, C,E, and F bands in Fig. 5 and for the D band in Fig. 6. The B band exhibits the same T dependence as the A band. The T dependences of the single-exciton bands are similar to each other except for the D band, which will be discussed separately below. When the temperature is raised from 4.5 K, the intensity increases monotonously with increasing temperature, passes through a broad maximum at 40—60 K, decreases and remains unchanged above 150 K. Such a T-dependence curve resembles the form predicted for magnon sidebands in antiferromagnetic crystals.[18,29] Therefore, it is suggested that the intensities of the observed single-exciton bands are given by the exciton-magnon interaction mechanism.

In the case of the D band (Fig. 6) measured using particular polarization, an anomalous increase of the intensity is observed when cooling below 25 K. Let us investigate what gives rise to this anomaly. A sharply polarized structure is observed in the D band as seen in Figs. 4(c) and 4(c'). Figure 4(c') shows the fine structure observed in the low-energy region using different propagation and polarization directions of the incident light. The peaks observed are named D_1,D_2,... in order of increasing energy, whose frequencies are listed in Table II. A sharp doublet-structured band (D_1 and D_2, their halfwidths are about 10 and 15 cm^{-1} at 5 K, respectively) is observed at the lowest-energy side of the D band. Unlike the structure observed in the high-energy region, the D_1 and D_2 peaks decrease rapidly and broaden with increasing temperature as shown in Fig. 7. The same behavior is also observed in the D_7 and D_8 peaks. Such temperature-sensitive peaks are not observed in the other single-exciton bands. For example, they are not observed even in the C band, which exhibits a rich fine structure [Figs. 4(b) and 4(b')]. As seen in Fig. 7, the D_2 peak slightly shifts toward the low-energy side with increasing temperature, while the red shift of the D_4 band is remarkably much larger. The T dependences of the peak positions of the D_2 and D_4 bands are plotted in Fig. 8, together with that of the E band. The D_2 peak does not shift at $T > T_N = 27$ K, while the D_4 peak shows a T dependence similar to that of the E peak, which is attributable to a magnon sideband. Therefore, from the T dependences of peak position and peak intensity, it is concluded that unlike the D_4 band, the D_1, D_2, D_7, and D_8 bands are not attributable to magnon sidebands.

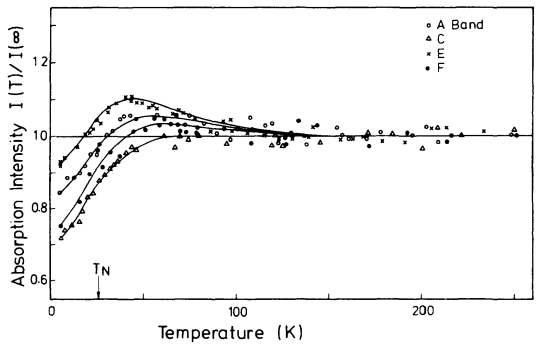

FIG. 5. Temperature dependence of the A-, C-, E-, and F-band intensities. The (a,c) plane and unpolarized light were used for the measurements of the A and C bands, whereas the (b,c) plane and $\vec{E}||c$ light refer to the results of the E and F bands.

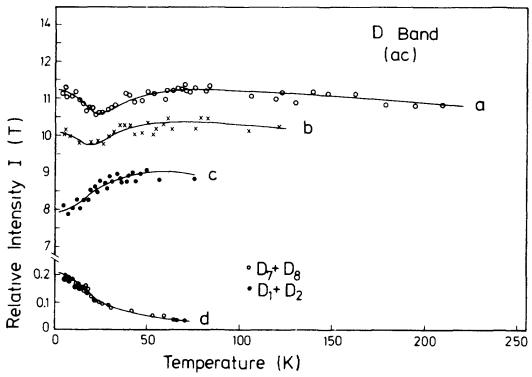

FIG. 6. Temperature dependence of the D-band intensity measured on the (a,c) plane using $\vec{E}||a$ (curve a), $\vec{E}||c$ (curve c), and unpolarized (curve b) lights, respectively. The total intensities of the D_1 and D_2 bands and of the D_7 and D_8 bands are shown in the bottom, which were measured on the (a,c) plane using $\vec{E}||c$ and $\vec{E}||a$ light, respectively. The two total intensities were accidentally identical within the experimental error, giving the same curve (d). The intensity scale for D_1+D_2 and D_7+D_8 is enlarged by a factor of 7.5.

In order to investigate the origin of the D_1, D_2, D_7, and D_8 bands, we measured the T dependence of the absorption intensity in the (a,c) plane using different polarization directions. The result is shown in curves a, b, and c of Fig. 6; the corresponding absorption spectra at 4.5 K are shown in curves a, b, and c of Fig. 9, respectively. As seen in Fig. 9, the intensity of the D_1, D_2, D_7, and D_8 bands is stronger in the $\vec{E}||a$ spectrum (curve a) than in the $\vec{E}||c$ spectrum (curve c), while the intensity is intermediate in the unpolarized spectrum (curve b) as expected. The total intensity of D_1+D_2 decreases with increasing temperature like that of D_7+D_8, as seen in curve d of Fig. 6.[30] Although an exact subtraction of $D_1+D_2+D_7+D_8$ from the total D band is difficult, it can be estimated that the T

TABLE II. Assignment of the fine structure in the D band. The energies of peak positions are obtained from the data at 5 K except for the D_1', D_2', and D_3' bands.

Band	Peak position (cm^{-1})	Assignment
D_3'	~27570[a]	three-magnon hot band associated with D_2 exciton
D_2'	~27633[a]	one-magnon hot band associated with D_1 exciton
D_1'	27651[b]	one-magnon hot band associated with D_2 exciton
D_1	27680	pure exciton
D_2	27697	pure exciton
D_3	27717	one-magnon cold band associated with D_1 exciton
D_4	27733	one-magnon cold band associated with D_2 exciton
D_5	~27745	
D_6	~27782	
D_7	27821	pure exciton
D_8	27850	pure exciton

[a]Obtained at 10 K.
[b]Obtained at 15 K.

dependence of the subtracted intensity remarkably resembles that of other single-excition bands such as the A band. Therefore, it is concluded that the D_1, D_2, D_7, and D_8 bands give rise to the low-temperature anomaly in the T dependence of the D-band intensity. In the following section we discuss the origin of the D_1, D_2, D_7, and D_8 bands.

C. Pyroelectric-moment–induced pure exciton absorption

An exciton is created at the center of the Brillouin zone (i.e., $\vec{k}=0$) by the optical absorption since the wavelength of the radiation is much larger than the lattice constant. So, although there may be a sizable exciton dispersion, the exciton band due to the $\vec{k}=0$ transition is expected to be very sharp. Indeed, sharp exciton bands have been observed at the lowest-energy side of absorption bands in various Mn^{2+} compounds, for example, in MnF_2 (Refs. 12 and 31) and $RbMnF_3$ (Ref. 32). We have observed two distinguishably sharp bands, D_1 and D_2, at the lowest-energy side of the D band. Therefore the D_1 and D_2 bands are attributable to exciton absorption. The exciton band observed in MnF_2 and $RbMnF_3$ has a very weak absorption intensity because of the magnetic dipole transition. Unlike the cases of

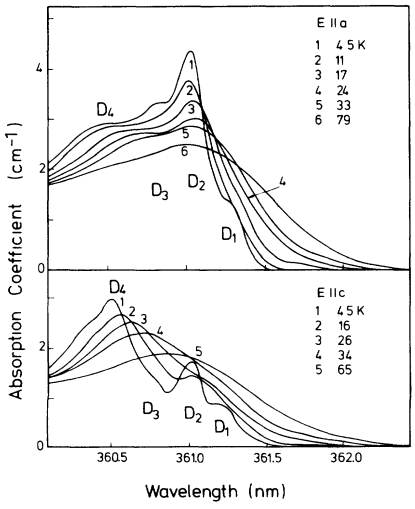

FIG. 7. D_1–D_4 band spectra at various temperatures measured on the (a,c) plane using $\vec{E}\|a$ (upper figure) and $\vec{E}\|c$ (bottom) light.

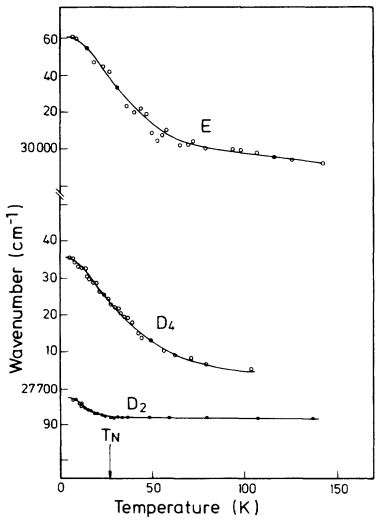

FIG. 8. Temperature dependence of the peak positions of the D_2, D_4, and E bands.

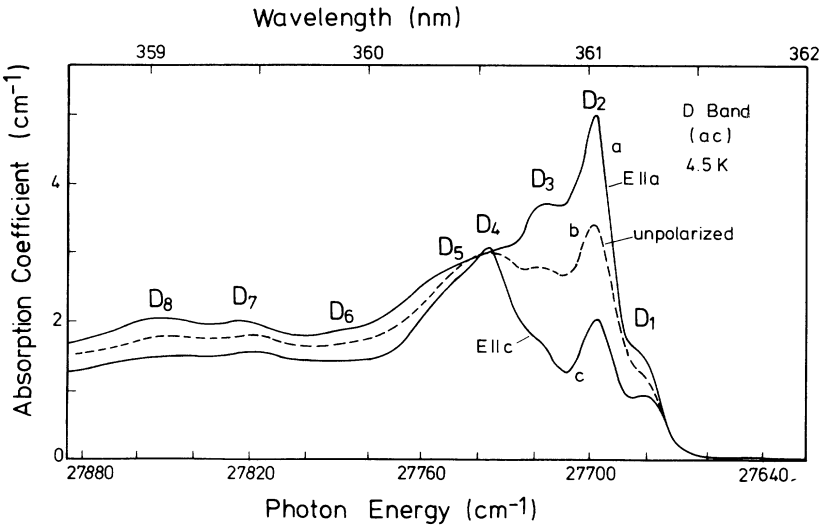

FIG. 9. Absorption spectra at 4.5 K of the D band measured on the (a,c) plane using $\vec{E}||a$ (curve a), $\vec{E}||c$ (curve c), and unpolarized (curve b) light, respectively.

MnF_2 and $RbMnF_3$, however, the intensities of the D_1 and D_2 bands are relatively large and not negligible in the whole D band. Related to this point, we now examine the D_1 and D_2 bands in detail.

A sharp doublet-structured absorption band, labeled D_1 and D_1', has been observed in the ${}^6A_{1g} \rightarrow {}^4T_{2g}$ (II) absorption band (D band) in the antiferromagnet $CsMnF_3$, which has been assigned to the electric-dipole-allowed pure exciton absorption.[14] When comparing our D_1 and D_2 bands with the D_1 and D_1' bands of $CsMnF_3$, several common features are found. For example, (i) in both cases these bands consist of sharp, intense doublets located at the low-energy side of the D band; (ii) both components are strongly polarized, depending on the $\vec{E}$ direction; (iii) when the temperature is increased from 5 K, both exhibit red shifts, which are much smaller than in the case of the magnon sideband; (iv) unlike the magnon sideband, both decrease their intensities as temperature is increased. Therefore it is suggested that our D_1 and D_2 bands are attributable to the electric-dipole-allowed pure exciton absorption. Another pure exciton absorption has also been observed in the high-energy region of the D band in $CsMnF_3$. This corresponds to our observation of the D_7 and D_8 bands, which were suggested to belong to the same origin as the D_1 and D_2 bands from their T dependence. Hence both D_1 and D_2, as well as D_7 and D_8, are proposed to be attributable to pure exciton absorption in $BaMnF_4$.

In the case of $CsMnF_3$, the dipole-allowed transition is connected with the existence of noncentrosymmetric Mn^{2+} sites. According to the x-ray analysis at room temperature,[1] each Mn^{2+} ion is surrounded by six F^- ions, forming a distorted MnF_6 octahedron, where the Mn^{2+} ion is located at a position that is noncentrosymmetric in the (a,b) plane but not along the $\vec{c}$ axis. From the structure of the distorted octahedra, it is expected that the $\vec{E}||a$ and $\vec{E}||b$ spectra of the pure exciton band should be quite similar to each other, but different from the $\vec{E}||c$ spectrum. When we closely investigate the dichroism of the D_1-D_2 structure shown in Fig. 4(c'), however, we find that the $\vec{E}||b$ spectrum is quite similar to the $\vec{E}||c$ spectrum, if we neglect their absolute intensities, whereas the $\vec{E}||a$ spectrum is quite different from the others. The dichroism in the D_1-D_2 region suggests the existence of a unique fourfold axis along the a-axis direction. Therefore, in the case of $BaMnF_4$, we must find an alternative reason for the appearance of a noncentrosymmetric Mn^{2+} site, which gives rise to the dipole-allowed pure exciton absorption. It is known that $BaMnF_4$ has a pyroelectric moment $\vec{P}$ directed along the a axis, that is, the Ba^{2+} ions produce a spontaneous electric polarization along the a axis.[3,5] The local electric field lies parallel to the direction of the a axis at the Mn^{2+}-ion site. Therefore it is suggested that this electric field polarizes the lattice and produces a polar distortion, resulting in a motion of the Mn^{2+} ion toward the final noninversion symmetric position along the a-axis direction. Although the

crystal symmetry of $BaMnF_4$ is known to be C_{2v}^{12} with only one twofold axis in the a-axis direction at room temperature, but not known at $T\sim 5$ K, we hereafter assume the site symmetry of Mn^{2+} ion at low temperatures ($T\sim 5$ K) to be approximately C_{4v} (the fourfold axis is along the a axis).

As shown in Fig. 4(c'), the intensity of the D_2 band is about twice that of the D_1 band in the $\vec{E}||b$ and $\vec{E}||c$ spectra. When the $\vec{E}$ direction is continuously changed from $\vec{E}||b$ or $\vec{E}||c$ into $\vec{E}||a$ in the (a,b) or (a,c) plane, respectively, it was observed that both bands grow monotonously and pass through neither maximum nor minimum. In the $\vec{E}||a$ spectrum the D_2-band intensity is about 3 times more intense than that of the D_1 band. A rigorous analysis of such a splitting and optical anisotropy of the pure exciton band associated with the ${}^6A_{1g}\rightarrow{}^4T_{2g}$ (II) transition requires knowledge of the energy levels and wave functions of the ${}^4T_{2g}$ (II) state in a C_{4v} crystal field, since the C_{4v} crystal field does not affect the ${}^6A_{1g}$ ground state because of its orbital singlet. The exchange field splits the ${}^6A_{1g}$ ground state into its six S_z components. The spin-orbit coupling between the levels of this multiplet vanishes, but the ${}^6A_{1g}$ state couples with the excited states such as ${}^4T_{1g}$ and ${}^4T_{2g}$ through spin-orbit interaction. The coupling with the lowest excited state ${}^4T_{1g}$ (I) is expected to be the strongest since the energy of the ${}^4T_{1g}$ (I) lies nearest to that of the ${}^6A_{1g}$ level. Therefore the ground state of the Mn^{2+} ion with $M_s=\frac{5}{2}$ is given by, using the first-order perturbation theory,

$$|{}^6A_{1g}(M_s=\tfrac{5}{2})\rangle = |{}^6A_{1g}(M_s=\tfrac{5}{2})\rangle - i\frac{\sqrt{5/2}\sigma_n}{E_0}|{}^4T_{1g},x(\tfrac{5}{2})\rangle + \frac{\sqrt{5/2}\sigma_n}{E_0}|{}^4T_{1g},y(\tfrac{3}{2})\rangle , \quad (2)$$

where σ_n represents the spin-orbit parameter and E_0 the energy distance between the ${}^6A_{1g}$ and ${}^4T_{1g}$ (I) levels.[31,33] Here $|{}^6A_{1g}\rangle$ means the ${}^6A_{1g}$ state mixed with the ${}^4T_{1g}$ state by spin-orbit interaction. Similarly, the ${}^4T_{2g}$ (II) level splits into four S_z components by the exchange field, ${}^4T_{2g}$ ($M_s=\frac{3}{2}$), ${}^4T_{2g}$ ($\frac{1}{2}$), ${}^4T_{2g}$ ($-\frac{1}{2}$), and ${}^4T_{2g}$ ($-\frac{3}{2}$) in order of increasing energy. The C_{4v} crystal field splits each of these levels into a doubly degenerate level ($T_{2g,\xi}$ and $T_{2g,\eta}$) and a nondegenerate level $T_{2g,\zeta}$ as shown in Fig. 10, where we take the ζ component in the a-axis direction. Here we assumed that the exchange field is stronger than the C_{4v} crystal field, i.e., $W_0>K$. If we take into account the spin-orbit coupling within the ${}^4T_{2g}$ (II) state, but neglect the coupling between the ${}^4T_{2g}$ (II) and other excited states, the final wave

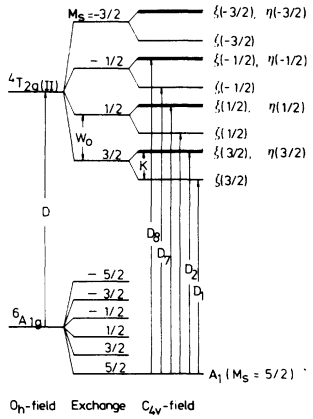

FIG. 10. Schematic energy-level diagram showing the ${}^6A_{1g}$ ground and ${}^4T_{2g}$ excited levels in the Mn^{2+} ion under the exchange and C_{4v}-symmetry crystal fields.

function is given as follows:

$$|\xi(M_s=\tfrac{3}{2})\rangle = |\xi(\tfrac{3}{2})\rangle + \frac{\lambda}{(W_0-K)\sqrt{2}}|\zeta(\tfrac{1}{2})\rangle ,$$

$$|\eta(M_s=\tfrac{3}{2})\rangle = |\eta(\tfrac{3}{2})\rangle - i\frac{\lambda}{(W_0-K)\sqrt{2}}|\zeta(\tfrac{1}{2})\rangle ,$$

$$|\zeta(M_s=\tfrac{3}{2})\rangle = |\zeta(\tfrac{3}{2})\rangle - \frac{\lambda}{(W_0+K)\sqrt{2}}|\xi(\tfrac{1}{2})\rangle + i\frac{\lambda}{(W_0+K)\sqrt{2}}|\eta(\tfrac{1}{2})\rangle ,$$

where ξ, η, and ζ mean $T_{2g,\xi}$, $T_{2g,\eta}$, and $T_{2g,\zeta}$, W_0 is the exchange-field splitting, K is the C_{4v} crystal-field splitting (see Fig. 10), and λ is the spin-orbit parameter of the T_{2g} state. The corresponding results are easily obtained for the other states such as $|\xi(M_s=\frac{1}{2})\rangle$. The transition from the ground state $|{}^6A_{1g}(\frac{5}{2})\rangle$ to these states are spin-orbit allowed because the quartet state is contained in the ground and excited states, but it is electric dipole forbidden because both states have the same even parity. The parity-forbidden electric dipole transition is slightly allowed by the presence of the static odd-parity of the C_{4v} crystal field, since the C_{4v}-symmetry static potential is given by[34]

$$V_{C_{4v}}=V_u(E_g)+V_\gamma(T_{1u}) . \quad (3)$$

The first term of Eq. (3) gives the level splittings as shown in Fig. 10, whereas the odd-parity field of the second term admixes even-parity states with odd-parity states, resulting in nonvanishing matrix elements of the electric dipole moment. The effective $\bar{\alpha}$-polarized ($\bar{\alpha}=\alpha,\beta,\gamma$) electric dipole transition moment $\vec{P}_{\rm eff}^{\bar{\alpha}}$ even-parity states m and n is proportional to the matrix $\langle m|V_{\rm odd}^{\bar{\alpha}}|n\rangle$.[34] The matrix is expressed, by the Wigner-Eckart thorem, as follows[34]:

$$\sum_{X,\bar{\xi}} \langle \Gamma_m || \bar{P}^X(\Gamma_u) || \Gamma_n \rangle \langle X\bar{\xi} \mid T_{1u,\bar{\alpha}} \Gamma_u \bar{\gamma} \rangle \times (\Gamma_m)^{-1/2} \langle \Gamma_m \mid \Gamma_n X\bar{\xi} \rangle ,$$

where $\langle \Gamma_m || \bar{P}^x(\Gamma_u) || \Gamma_n \rangle$ is the so-called reduced matrix, $\Gamma_u \bar{\gamma}$ is the irreducible representation of the odd-parity potential (in the present case $\Gamma_u \bar{\gamma} = T_{1u}\gamma$), and (Γ_m) denotes the dimension of the irreducible representation Γ_m. By calculating the above Clebsch-Gordan coefficients, one can obtain the selection rule for the ${}^6A_{1g} \rightarrow {}^4T_{2g}$ (II) transition.

Six absorption bands are expected as the result of electric dipole transition from the ground state of Eq. (2) as shown by arrows in Fig. 10. The intensity ratio of the first band associated with the ${}^6A_{1g} \rightarrow \zeta(\frac{3}{2})$ transition to the second band associated with the ${}^6A_{1g} \rightarrow \xi(\frac{3}{2}), \eta(\frac{3}{2})$ transitions is given by $\lambda^2/2(W_0+K)^2$:1 in the $\vec{E}||a$ polarization, whereas $1:\lambda^2/(W_0-K)^2$ in the $\vec{E}||b$ or $\vec{E}||c$ polarization. If we assign the first band to the D_1 band and the second band to the D_2 band (see Fig. 10), the experimental results give the values $K=17$ cm^{-1} and $W_0=65$ cm^{-1}. With the use of this W_0 value, the fifth band associated with the ${}^6A_{1g} \rightarrow \zeta(-\frac{1}{2})$ transition is estimated to be located at 130 cm^{-1} ($=2W_0$, see Fig. 10) from the first band, which is quite close to the position of the D_7 band lying 141 cm^{-1} from the D_1 band. The third band associated with the ${}^6A_{1g} \rightarrow \zeta(\frac{1}{2})$ transition is estimated to be at a distance of another 65 cm^{-1}. This position lies in the spectral region of the intense and broad magnon sideband D_4; therefore it is expected to be difficult to observe. This is consistent with the experiment.

The D_1 and D_2 bands are observed to be more intense in the $\vec{E}||a$ spectrum than in the $\vec{E}\perp a$ spectrum. This is qualitatively in agreement with our identification of these bands as now outlined. For example, according to our calculation with respect to the second band, the intensity ratio of the $\vec{E}||a$ polarized spectrum to the $\vec{E}\perp a$ polarized spectrum is given by

$$\langle T_{2g} || \bar{P}^{E_g} || T_{1g} \rangle^2 : | \langle T_{2g} || \bar{P}^{T_{2g}} || T_{1g} \rangle - \langle T_{2g} || \bar{P}^{T_{1g}} || T_{1g} \rangle |^2 .$$

It seems to be probable that the two reduced matrices $\langle T_{2g} || \bar{P}^{T_{2g}} || T_{1g} \rangle$ and $\langle T_{2g} || \bar{P}^{T_{1g}} || T_{1g} \rangle$ have almost the same magnitude since the three-dimensional T_{2g} and T_{1g} irreducible representations are expected to give an almost equivalent contribution to the reduced matrix of P. Therefore, the amount of

$$| \langle T_{2g} || \bar{P}^{T_{2g}} || T_{1g} \rangle - \langle T_{2g} || \bar{P}^{T_{1g}} || T_{1g} \rangle |^2$$

is expected to be considerably smaller than that of $\langle T_{2g} || \bar{P}^{E_g} || T_{1g} \rangle^2$, in agreement with the experimental result on the D_2 band. In Fig. 10 we summarize the assignment of the D_1, D_2, D_7, and D_8 transitions.

D. Three-magnon hot band

In the two-sublattice antiferromagnets, the magnon sideband consists of so-called cold and hot bands around the pure exciton band. The cold band is expected to appear at $W_{ex}+W_{mag}$ (one-exciton and one-magnon process), if we neglect the exciton-magnon interaction, whereas the hot band appears at $W_{ex}-W_{mag}$ (one-exciton and one-magnon process, called one-magnon hot band) and $W_{ex}-3W_{mag}$ (one-exciton and three-magnon process called three-magnon hot band), where W_{ex} and W_{mag} are energies of excitons and magnons respectively.[18,35] The zone-boundary magnon energy in $BaMnF_4$ has been calculated as $W_{mag}=46$ cm^{-1} by Moncorgé and Jacquier.[9] We believe that this value is reliable, being consistent with the magnon dispersion measured by neutron scattering.[36] A cold band observed in the A-band excitation spectrum appears at 38 cm^{-1} at the high-energy side of the exciton band,[9] which is displaced by the exciton-magnon interaction of 8 cm^{-1} in the D band. The magnon sidebands D_3 and D_4 appear at 37 and 36 cm^{-1} from the D_1 and D_2 pure exciton bands, respectively, which are quite close to the above 38 cm^{-1}. Therefore, the D_3 and D_4 bands are attributable to the cold bands associated with the D_1 and D_2 bands, respectively. The cold bands are expected to appear more intensely at $T=0$, whereas the hot bands should appear only at $T\neq 0$ with a tendency of growing with increasing temperature.[37] To find the hot band, therefore, the T dependence of the absorption spectrum around the pure exciton band should be first investigated.

As shown in Fig. 11, three weak absorption bands are observed at the low-energy tail of the D_1 band above 13 K, all the bands growing with increasing temperature. We call them D_1', D_2', and D_3' bands in order of decreasing energy. Their peak energies are collected in Table II. The D_1-D_2' separation is about 46 cm^{-1} at 13 K, which is almost equal to the D_2-D_1' separation. It has been suggested that the exciton-magnon interaction energy is smaller in the hot band than in the cold band,[12,14] which leads to the result that the distance from the pure exciton band is larger for the hot band than for the cold band. Taking into account this point, we arrive at the conclusion that the D_1' and D_2' bands are attributable to the one-magnon hot bands associated with the D_2 and D_1 pure exciton bands, respectively.

To the authors' knowledge, to date three-magnon

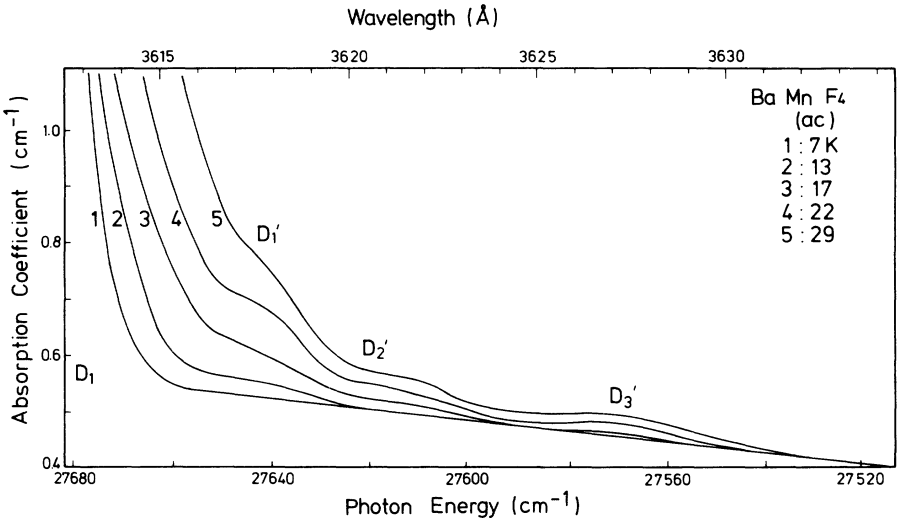

FIG. 11. Unpolarized absorption spectra at the low-energy tail of the D_1 band measured on the (a,c) plane at various temperatures.

hot bands have never been observed in absorption spectra clearly. $BaMnF_4$ seems to be suitable to show their existence. The D_3' band appears at about 124 cm^{-1} from the D_2 pure exciton band at 13 K, which is about 3 times that of the D_2-D_1' separation. Furthermore, we have plotted the absorption-peak intensities of the D_1' and D_3' bands against temperature in Fig. 12. The behavior of their relative intensities is quite similar to the theoretically calculated T dependences of three-magnon and one-magnon hot bands (see Fig. 4 of Ref. 37). From these facts the D_3' band is attributable to the three-magnon hot band associated with the D_2 pure exciton band. Another three-magnon hot band, associated with the D_1 band, is expected at the low-energy side of the D_3' band but not observed clearly because of the weak intensity proportional to the original D_1 band. In Table II we summarize the assignment of the observed pure exciton band and magnon sideband.

E. Optical detection of three-dimensional spin ordering

$BaMnF_4$ is known as a two-dimensional (2d) antiferromagnetic material because of its layered crystal structure. It, however, was shown by magnetic susceptibility measurements that a three-dimensional (3D) behavior appears below T_N, as mentioned in Sec. I. Here we try to confirm the appearance of three dimensionality optically. To do so, we compare the spectroscopic data of $BaMnF_4$ with the theoretical calculation derived for one-, two-, or three-dimensional antiferromagnetic Mn^{2+} compounds. So far such a theoretical calculation has been done for magnon sidebands in one-dimensional (1D) and 3(D) antiferromagnets,[18,29,35–38] but not for the 2D case. Therefore, for the 2D case we tentatively use the experimental result of the layered compounds $(C_2H_5NH_3)_2MnCl_4$ ethyl-ammonium-manganese-chloride (EAMC) and $(C_3H_7NH_3)_2MnCl_4$ propyl-ammonium-manganese-chloride (PAMC)[39] for comparison.

1. Integrated intensity of magnon sidebands

As seen in Fig. 5 a common feature occurs in the T dependences of the A-, B-, C-, E-, and F-band intensities, although slight differences are observed among these bands: The integrated intensity increases with rising temperature from 4.5 K, approaches a maximum value between 45 and 60 K, gradually decreases and, above about 150 K, it takes a constant value which is larger than I ($T=4.5$ K). Such a T-dependence curve is, unfortunately, found in common to all 1D, 2D, and 3D antiferromagnets,

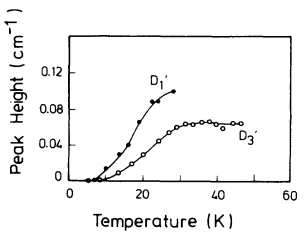

FIG. 12. Temperature dependence of the maximum absorption coefficients of the D_1' and D_3' bands.

and therefore it does not indicate a special dimensionality clearly. However, characteristic differences among the three cases are found in the value of T_{max} relative to T_N; one finds $T_{max} \gg T_N$ for the 1D case (e.g., $T_{max}/T_N \approx 70$ for tetramethyl-ammonium-manganese-chloride TMMC), $T_{max} > T_N$ for the 2D case (e.g., $T_{max}/T_N \approx 1.5$ in EAMC and PAMC), and $T_{max} \approx T_N$ for the 3D case. In $BaMnF_4$, T_{max}/T_N takes a value between 1.6 and 2.0 depending on the absorption band. From this view we can confirm the presence of 2D spin order in $BaMnF_4$.[40] According to the theoretical T dependence[37] which was calculated for 3D $RbMnF_3$ with $T_N = 83$ K, an almost temperature independent intensity is found between 0 and 40 K. In our case it is difficult to find such a character below T_N although 3D ordering appears in the low-temperature region. This is consistent with the idea that 3D ordering is only a marginal effect in $BaMnF_4$, which exhibits preponderantly 2D spin correlations of the Heisenberg type.[41]

2. Peak energy

According to the calculation on 3D $RbMnF_3$,[37] the peak energy of the magnon sideband is almost independent of temperature at low temperatures near 0 K, and, as temperature is raised, it decreases with temperature and then reaches a constant value. A very weak maximum is superimposed at T_N (see Fig. 9 of Ref. 37). A similar T dependence is observed for 2D EAMC and PAMC, but the temperature-independent region extends until near T_N and no singularity is observed at T_N.[39] The behavior of the peak shift observed in the D_4 magnon sideband (Fig. 8) seems to correspond to the 3D case at low temperatures rather than to the 2D case, since the temperature-independent region observed around $T = 0$ is very narrow. Thus the 3D character seems to appear prominently at low temperatures although an expected weak singularity is not observed clearly at $T = T_N$.

3. Halfwidth

When the temperature is raised from 0 K, the calculated halfwidth $W(T)$ of the cold band in 3D $RbMnF_3$ increases in proportion to a T^2-like function and reaches a maximum at $T = T_N$, and then decreases gradually to become constant at high temperatures.[37] On the other hand, the theoretical halfwidth of 1D TMMC exhibits a T dependence of a $T^{1/2}$-like function, that is, it increases monotonously with temperature without a singularity at T_N and takes a constant value at high temperatures.[29] It is difficult to measure the halfwidth of the magnon sidebands in $BaMnF_4$ precisely, because the magnon sidebands observed in the D band are not well resolved. A simple line shape is found in the E band, which consists of two broad bands, E_1 and E_2, peaking at 332.8 and 329 nm at 4.5 K. Each line shape is believed to be an envelope formed from the superposition of many unresolved magnon sidebands. In curve a of Fig. 13 we show the T dependence of the halfwidth of the E_1 band. The halfwidth increases gradually with increasing temperature in the low-temperature region, which is similar to the 3D case, changes the rate of increasing at about 45 K, and increases very slowly in the high-temperature region just as in the 1D case. Thus although neither theoretical nor experimental curves to be compared with our curve have been given on the halfwidth in 2D antiferromagnets, it seems that the 3D character appears weakly at low temperature, as is expected.

In order to find a symptom of three dimensionality in $BaMnF_4$ clearly, we choose the D_2 band, which is so strong and well resolved that it is easy to measure the halfwidth. Unfortunately, the D_2 band is not a magnon sideband but a pure exciton band. Neither theoretical nor experimental studies have been made on the halfwidth of a pure exciton band in the 2D or 3D antiferromagnet. We can expect that, as temperature is increased, interactions with phonons and magnons will affect the exciton line, for example, giving rise to broadening. At low temperatures below T_N, the effect of magnons (i.e., exchange interaction) is expected to be stronger than that of phonons in antiferromagnets, giving rise to the same phenomenon as in the case of the magnon sideband. Indeed, similar effects of exchange interaction have been observed on the peak shift of both the magnon sideband and pure exciton band in $CsMnF_3$.[14,15]

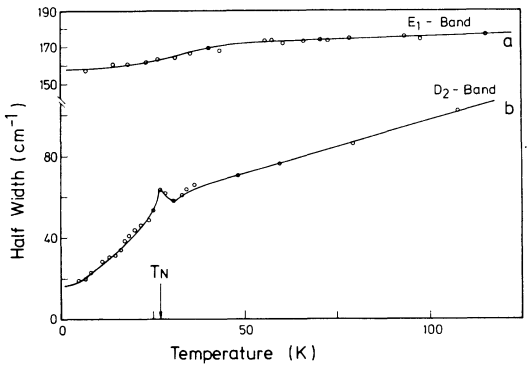

FIG. 13. Temperature dependence of the half-width of the E_1 (curve a) and D_2 (curve b) bands measured on the (b,c) and (a,c) planes using $\vec{E}||c$ and $\vec{E}||a$ light, respectively.

We find a marked cusp at T_N in the halfwidth of the D_2 band as shown in Fig. 13 (curve *b*). Such a cusp is found in the theoretical T dependence of the halfwidth of the magnon cold band in 3D $RbMnF_3$.[37] The cusp at T_N may be interpreted by the exchange splitting of the ground state due to the spontaneous onset of the long-range exchange field due to 3D interactions at T_N and the subsequent depletion of the magnon states on lowering the temperature. Moreover, we find that the T-dependence curve of the D_2 band up to $T=T_N$ is similar to theoretically[37] calculated T dependence in the low-temperature region up to T_N. Thus we can find the presence of 3D spin ordering to $BaMnF_4$ from the pure exciton band. Unlike the case of magnon sidebands in purely 3D $RbMnF_3$, however, the singularity is not so prominent, suggesting that the three dimensionality is not so pronounced as is expected for $BaMnF_4$.

F. Luminescence

Goldberg *et al.* observed three broad emission bands peaking at about 600, 640, and 720 nm in $BaMnF_4$, which disappear above 110 K, and assigned them to the emission from Mn^{2+} ions perturbed by nearby impurity ions.[8] Such an impurity-induced luminescence has been observed in other Mn^{2+} compounds.[42] Since the impurity-perturbed Mn^{2+} ions have the excited energy levels below the lowest excited level $^4T_{1g}$ (I) of the pure Mn^{2+} ion, these ions can act as traps of mobile excitons originated from unperturbed Mn^{2+} ions. The trapped excitation energy is released as luminescence, which is characteristic of the individual perturbed Mn^{2+} ion. As the temperature is raised, a shallow trap can no longer retain the excitation energy and releases it into the crystal by thermal agitation, resulting in a decay of the luminescence characteristic of the shallow trap. The released excitation energy is believed to be either transferred to deeper traps, producing another luminescence, which is characteristic of the deep traps, or quenched during the diffusion of excitation energy by nonradiative multiphonon processes.[42] The 600-nm emission of $BaMnF_4$ was reported to have a maximum intensity at about 10 K.[8] This temperature is interpreted as a critical temperature, which gives a measure of trapping or detrapping of excitation energy by the localized trap. Here we investigate the 600-nm emission in detail to make sure of the existence of such a shallow trap in $BaMnF_4$.

Figure 14 shows the emission spectra produced by the excitation in the *A* band at various temperatures. The same spectra were also obtained by the *B*- or *C*-band excitation. As the temperature is raised from 4.5 K, the 600-nm emission band grows gradually,

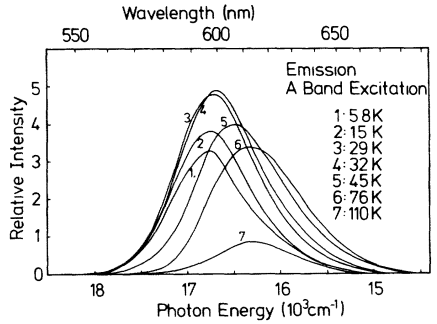

FIG. 14. Emission spectra produced by the excitation in the *A* band at various temperatures. Unpolarized light was irradiated on the (*b*,*c*) plane and luminescence emitted from the (*a*,*c*) plane was detected. A Philips 150 UVP photomultiplier was used as detector, which has appreciable sensitivity only at the high-energy side of 650 nm.

has a maximum intensity at about 33 K, decreases gradually until about 60 K, but rapidly from 80 K, and disappears at about 130 K as shown in Fig. 15. Unlike the observation made by Goldberg *et al.*,[8] the 600-nm emission is not observed to have a maximum intensity at about 10 K. It is noticed that the T-dependence curve of the emission intensity is quite similar to that of absorption intensity (Fig. 5) in a temperature region below 60 K, where antiferromagnetic spin ordering appears. Such a T dependence has never been observed in both 2D and 3D antiferromagnetic Mn^{2+} compounds.[43,44] Our T dependence is interpreted as follows. In the antiferromagnetic phase the excitation energy is localized and not diffused into the crystal, because exciton transfer into nearest neighbors by spin-exchange in-

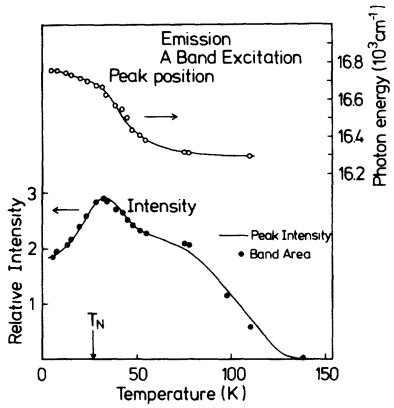

FIG. 15. Temperature dependence of intensity (band area), peak height (curve *a*), and peak position (curve *b*) of the 600-nm emission band produced by the *A*-band excitation. The band area is plotted so as to coincide at its maximum with the maximum in the curve of the peak height. It is seen that the band-area points follow the curve of the peak height (peak intensity) quite well.

teraction is not allowed between two antiparallel magnetic moments.[9,11] The Mn^{2+} ions, which are near impurity-perturbed Mn^{2+} ions, however, transfer the excitation energy into the nearby perturbed Mn^{2+} ions since the antiferromagnetic coupling between two Mn^{2+} ions is relaxed around the impurity ions. Thus the excitation energy released by the pure Mn^{2+} ions is trapped by the perturbed Mn^{2+} ions via the short-range transfer and used to produce the luminescence. In such a short-range transfer it is believed that the intensity absorbed by the pure Mn^{2+} ions is nearly directly (i.e., without an appreciable loss along the migration path) transferred into the nearby traps. Therefore the emission intensity reflects the original absorption intensity, i.e., the T-dependence curves of both intensities are similar to each other below 60 K. On the other hand, in $BaMnF_4$ the exchange-induced exciton transfer among pure Mn^{2+} ions is not negligible below T_N, because a weak ferromagnetic moment arises due to a slight canting of the spins.[3] Hence the presence of long-range exciton transfer modifies the one-to-one relationship between the emission and absorption intensities. Indeed, the T_{max} of the emission intensity is observed to shift by about 10 K from T_{max} of the absorption intensity.

As seen in Fig. 15, the T-dependence curve of the 600-nm emission intensity no longer resembles that of the absorption intensity above 70 K. This indicates an influence of lattice vibrations, which give rise to quenching of the luminescence. The effect of lattice vibrations is also seen in the peak shift of the 600-nm emission band. As shown in Fig. 15, the peak position of the 600-nm emission band shifts towards lower energy with increasing temperature. The rate of the red shift is small below 30 K but increases rapidly above about 40 K. The peak shift between 5 and 80 K amounts to about 450 cm^{-1}. Such a large shift cannot be explained by the exciton-magnon interaction only. The electron-phonon interaction plays an important role for the peak shift as in the case of the 2D antiferromagnet EAMC.[44] The experimental result that the vibrational effect appears obviously above 70 K is also in agreement with the linear birefringence measurements.[45]

IV. DISCUSSION

As mentioned in Sec. III B, the optical anisotropy of the exciton absorption bands have been pretty well understood within the framework of the so-called single-ion (one-ion) electric dipole mechanism. Atlhough the effect of the spin-exchange interaction mechanism between two Mn^{2+} ions (two-ion process) is not negligible for the exciton band as seen in Sec. III E 3, we can show, from the T dependence of pure exciton absorption intensity, that such a one-ion process is not an unreasonable assumption for $BaMnF_4$. According to the calculation on the zero-magnon (i.e., exciton) line intensity in antiferromagnets,[46] (i) in the one-ion process, where exciton absorption is electric dipole allowed by odd crystal field and spin-orbit interaction as in our case, the intensity has a maximum value at $T=0$, being invariable in the temperature region of $0<T<0.3T_N$, but decreases gradually as the temperature is increased up to T_N; whereas (ii) in the two-ion process, the intensity is zero at $T=0$, increases as the temperature is increased, has a broad maximum near T_N, and decreases as the temperature approaches T_N. The T dependence of the exciton band observed in Cr_2O_3 has been explained using a mixture of these two processes.[46] A T dependence similar to the case of Cr_2O_3 has also been observed for exciton bands in $CsMnF_3$.[14] We believe that the T dependence of $CsMnF_3$ is also understood by a competition of these two processes just as in the case of Cr_2O_3.

On the other hand, the T dependence of the intensity of the pure exciton bands in $BaMnF_4$ is quite similar to the theoretical curve derived under the one-ion process.[46] The spin-exchange interaction J between two magnetic ions is $|J|=60$ cm^{-1} for Cr_2O_3,[46] whereas $|J_c|$ (along the c direction) $=4.7$ cm^{-1} and $|J_a|$ (along the zigzagging a direction) $=3.4$ cm^{-1} for $BaMnF_4$.[36] The J value is, hence, considerably smaller in $BaMnF_4$ than in Cr_2O_3, suggesting that the two-ion process is more important in Cr_2O_3 than in $BaMnF_4$, since the exchange interaction must be strong for the appearance of the two-ion process. Therefore our suggestion that the contribution of the two-ion process is less prominent than that of one-ion process is confirmed to be reasonable.

Next we discuss the dichroism observed in the single-exciton bands obtained in $\vec{E}||a$, $\vec{E}||b$ and $\vec{E}||c$ spectra. From Table I we find that the values of f_a, f_b, and f_c are almost comparable with each other for the A, B, D, and F bands (called type-I bands hereafter), whereas the f_c value is much larger than the f_a or f_b value for the C, E, and G bands (type-II bands). In order to understand the optical anisotropy depending on the band, we first consider the site symmetry around a Mn^{2+} ion. Each Mn^{2+} ion of $BaMnF_4$ has two nearest-neighboring Mn^{2+} ions along the c axis, two Mn^{2+} ions in the (a,c) plane, and two Mn^{2+} ions along the b axis. Thus the central Mn^{2+} ion has the site symmetry C_{2v} with a two-fold axis along the c axis, if six F^- ions associated with each Mn^{2+} ion are assumed to form a regular octahedron. Under the C_{2v} local symmetry the $^4T_{1g}$

level responsible for the A and F bands splits into $^4A_2$, $^4B_1$, and $^4B_2$ levels, and the $^4T_{2g}$ level responsible for the B and D bands has the same splitting as the $^4T_{1g}$ level, whereas the ^4E_g level responsible for the C and E bands splits into two $^4A_1$ levels. We find that the excited states responsible for type-I bands consist of the $^4A_2$, $^4B_1$, and $^4B_2$ states, whereas those for type-II bands merely consist of the same two or three $^4A_1$ states. Therefore, from the experimental result that all the bands belonging to type I exhibit similar optical anisotropy and the same is true for the type-II bands, it is suggested that the anisotropy of the single-exciton band is predominantly determined by the kind of excited state, although it is necessary for the calculation of oscillator strength to take into account the complicated selection rules for exciton-magnon, exciton-phonon, and exciton-magnon-phonon transitions[47] involved in a single-exciton band. Indeed, this suggestion is supported by another experimental result that the anisotropy is different between types I and II, since the A_1 electronic state responsible for the type-II bands is polarized parallel to the c axis, whereas the B_1 and B_2 states responsible for the type-I bands are polarized perpendicularly to the c axis.

Here we try to find a reason why the f_a, f_b, and f_c values of the type-I band are approximately equal to each other. The electronic transition from the ground state $^6A_{1g}$ ($^6A_1$ in C_{2v} symmetry) to the excited states of the A—G bands is spin forbidden, but, since the practical ground state contains the $^4T_{1g,\alpha}$ ($^4B_1$ in C_{2v} symmetry) and $^4T_{1g,\beta}$ ($^4B_2$) states as mentioned in Sec. III B, the transition becomes allowed. Taking into account the selection rule for the electric dipole transition in C_{2v} symmetry (for example, the $^4B_1 \rightarrow {}^4A_1$ transition is allowed for $\vec{E} \perp c$ polarization), all the type-I bands are allowed for both $\vec{E} \| c$ and $\vec{E} \perp c$ polarizations, whereas all the type-II bands are allowed for only $\vec{E} \| c$ polarization. The former result is consistent with the experiment qualitatively, but the latter result is not successful in explaining the appearance of a distinguishably large f_c value. This indicates a limit in the use of the single-ion (not exchange induced) electric dipole mechanism for the type-II bands.

V. CONCLUSIONS

We note the following. (1) The entire absorption spectrum of the pyroelectric antiferromagnet $BaMnF_4$ observed in the visible-ultraviolet region is quite similar to that of usual antiferromagnets like MnF_2 and $RbMnF_3$; the spectrum consists of seven single-exciton bands associated with a Mn^{2+} ion and three double-exciton bands. In most Mn^{2+} compounds, the one-ion pure exciton transitions associated with $d^5 \rightarrow d^5$ electronic transitions of Mn^{2+} are parity forbidden, since the Mn^{2+} ions lie at a center of inversion, and therefore weak magnetic dipole transitions are responsible for the pure exciton absorption observed so far. The two-ion exciton-magnon process, where the magnon disturbs the inversion symmetry and induces an electric dipole transition, not for a Mn^{2+} monomer center but for a Mn^{2+} dimer center, plays a very important role in inducing a strong absorption intensity for the single- and double-exciton bands. It has been nearly twelve years since an electric-dipole-allowed pure exciton absorption band in Mn^{2+} compounds was first found in $CsMnF_3$ by Belyaev *et al.*[13] We found an electric-dipole-allowed exciton absorption in a single-exciton band (D band) in $BaMnF_4$, from the observation of an unusual temperature dependence of the D-band intensity. From the investigation of the optical anisotropy of the pure exciton band, we found that the noncentrosymmetric position of Mn^{2+} ions, which is responsible for the appearance of the exciton band, is produced by the pyroelectric moment induced by Ba^{2+} ions; that is to say, the existence of the anisotropy of the pure exciton band is explained as being due to pyroelectricity.

(2) The three-magnon hot band has been theoretically predicted to appear in antiferromagnets, but it has not been observed yet. We found the three-magnon hot band at the low-energy side of the one-magnon hot band, which appears at the low-energy tail of the pure exciton band observed in the D band. The estimated magnon energy is consistent with the magnon dispersion obtained by neutron scattering.

(3) The appearance of three-dimensional spin ordering, which has been suggested from the magnetic susceptibility measurements, has been optically confirmed from the temperature dependence of the integrated intensity and peak energy in the magnon sideband and of the halfwidth of the pure exciton band. However, the observed three-dimensional character is quite weak and superimposed on the two-dimensional character. This is consistent with the fact that $BaMnF_4$ has a layered crystal structure and therefore is expected to exhibit two-dimensional behavior predominantly.

(4) The temperature dependence of the 600-nm emission intensity in the low-temperature region of $T < 60$ K has been observed to be quite similar to that of the single-exciton band intensity. This is understood by an involvement of a short-range excitation-energy transfer mechanism, which occurs between Mn^{2+}-ion sites and nearby impurity-associated Mn^{2+}-ion sites.

ACKNOWLEDGMENTS

The experimental part of this work was undertaken when one of the authors (T.T.) was staying at the Universität—Gesamthochschule Paderborn. He sincerely thanks the Universität—Gesamthochschule Paderborn, for its hospitality and the Ministry of Science and Research, Nordrhein-Westfalen (Federal Republic of Germany), for providing a guest professorship during this stay. Thanks are due to M. Régis for the loan of one sample of $BaMnF_4$ used in our preliminary experiments. We are greatly indebted for D. Niggemeyer, who grew the crystals, and to F. J. Schäfer for orienting and polishing the samples.

---

*Visiting professor at Universität—GH-Paderborn in 1981–82.

†Present address: Fachbereich 10 (Angewandte Physik), Universität—GH-Duisburg, 4100 Duisburg, Federal Republic of Germany.

[1]E. T. Keve, S. C. Abrahams, and J. L. Bernstein, J. Chem. Phys. 51, 4928 (1969).

[2]L. M. Holmes, M. Eibschütz, and H. J. Guggenheim, Solid State Commun. 7, 973 (1969).

[3]An excellent review is given by J. F. Scott, Rep. Prog. Phys. 12, 1055 (1979).

[4]Recent work has been done by K. B. Lyons, R. N. Bhatt, T. J. Negran, and H. J. Guggenheim, Phys. Rev. B 25, 1791 (1982); J. F. Scott, F. Habbel, and M. Hidaka, *ibid.* 25, 1805 (1982).

[5]D. R. Tilley and J. F. Scott, Phys. Rev. B 25, 3251 (1982).

[6]M. Régis, M. Candille, and P. St.-Grégoire, J. Phys. (Paris) Lett. 41, L-423 (1980).

[7]P. St.-Grégoire, Ph.D. Thesis, Université de Montpellier, 1981 (unpublished).

[8]V. Goldberg, D. Pacheco, R. Moncorgé, and B. Di Bartolo, J. Lumin. 18/19, 145 (1979).

[9]R. Moncorgé and B. Jacquier, Phys. Lett. 85A, 390 (1981).

[10]See, for example, V. V. Eremenko, Adv. Phys. 26, 31 (1977).

[11]D. S. McClure, in *Optical Properties of Ions in Solids,* edited by B. Di Bartolo (Plenum, New York, 1975), p. 259.

[12]R. S. Meltzer, M. Lowe, and D. S. McClure, Phys. Rev. 180, 561 (1969).

[13]A. I. Belyaea, V. V. Eremenko, V. I. Silaev, and S. V. Petrov, Zh. Eksp. Teor. Fiz. 58, 475 (1970) Soviet Phys. JETP 31, 253 (1970).

[14]A. I. Belaea, V. S. Kuleshov, V. I. Silaev, and N. V. Gapon, Zh. Eksp. Teor. Fiz. 61, 1492 (1971) [Sov. Phys.—JETP 34, 794 (1972)].

[15]B. Jacquier, R. Moncorgé, and B. Di Bartolo, Solid State Commun. 31, 693 (1979).

[16]J. Ferguson, Aust. J. Chem. 21, 307 (1968).

[17]S. E. Stokowski and D. D. Sell, Phys. Rev. B 3, 208 (1971); S. E. Stokowski, D. D. Sell, and H. J. Guggenheim, *ibid.* 4, 3141 (1971).

[18]T. Fujiwara, W. Gebhardt, K. Petanides, and Y. Tanabe, J. Phys. Soc. Jpn. 33, 39 (1972).

[19]J. Ferguson, H. J. Guggenheim, and Y. Tanabe, J. Phys. Soc. Jpn. 21, 692 (1966).

[20]R. H. Petit, J. Ferré, and J. Nouet, Physica (Utrecht) 86-88B, 1213 (1977).

[21]W. Kleemann, F. J. Schäfer, and J. Nouet, J. Phys. C 14, 4447 (1981).

[22]J. Ferguson, H. J. Guggenheim, and Y. Tanabe, Phys. Rev. 161, 207 (1967).

[23]J. W. Stout, J. Chem. Phys. 31, 709 (1959).

[24]Y. Tanabe and S. Sugano, J. Phys. Soc. Jpn. 9, 753 (1954).

[25]A. K. Mehra, J. Chem. Phys. 48, 4384 (1968).

[26]J. L. Rao and K. Purander, Solid State Commun. 37, 983 (1981).

[27]T. Fujiwara, J. Phys. Soc. Jpn. 34, 1180 (1973).

[28]M. Eibschütz and H. J. Guggenheim, Solid State Commun. 6, 737 (1968); F. J. Schäfer (private communication).

[29]K. Ebara and Y. Tanabe, J. Phys. Soc. Jpn. 36, 93 (1974).

[30]We chose the $\vec{E}||c$ ($\vec{E}||a$) spectrum for the D_1+D_2 (D_7+D_8) intensity measurement, because subtracting the background is easier than in other spectra.

[31]D. D. Sell, R. L. Greene, and R. M. White, Phys. Rev. 158, 489 (1967).

[32]M. Y. Chen, D. S. McClure, and E. I. Solomon, Phys. Rev. B 6, 1960 (1972); E. I. Solomon and D. S. McClure, *ibid.* 9, 4690 (1974).

[33]S. Koide and M. H. L. Pryce, Philos. Mag. 3, 607 (1958).

[34]S. Sugano, Y. Tanabe, and H. Kamimura, *Multiplets of Transition-Metal Ions in Crystals* (Academic, New York, 1970); H. Kamimura, S. Sugano, and Y. Tanabe, *Introduction to Ligand Field Theory* (Shokabo, Tokyo, 1969) (in Japanese).

[35]K. Shinagawa and Y. Tanabe, J. Phys. Soc. Jpn. 30, 1280 (1971).

[36]D. E. Cox, S. M. Shapiro, R. A. Cowley, M. Eibschütz, and H. J. Guggenheim, Phys. Rev. B 19, 5754 (1979).

[37]T. Fujiwara and Y. Tanabe, J. Phys. Soc. Jpn. 32, 912 (1972).

[38]H. Tanaka, J. Phys. Soc. Jpn. 31, 368 (1971).

[39]N. Kojima, T. Ban, and I. Tsujikawa, J. Phys. Soc. Jpn. 44, 919 (1978).

[40]$BaMnF_4$ has a similiar layered crystal structure as EAMC and PAMC. The maximum intensity locates at $T_{max} \approx 1.5JS(S+1)k_B$ in EAMC and PAMC for the single-exciton band corresponding to our C band (Ref. 39), where J is intralayer spin-exchange interaction in

the (a,c) plane. Unlike EAMC and PAMC with almost ideally square layers (i.e., $a \approx c$, a and c denote lattice constants in the a- and c-axis directions), two kinds of intralayer exchange interactions, J_a and J_c, are present in $BaMnF_4$ because $a < c$, where J_a and J_c refer to the exchange parallel to the zigzagging a and the c directions, respectively; of course, the J_a value is different from J_c value (Ref. 36). This seems to cause the appearance of different observed T_{max} values, e.g., for the E and F bands we have noted that the maximum intensity seems to lie at a unique value $T_{max} \sim 2.0JS(S+1)/k_B$, if $J = J_a$ applies to the E band, whereas $J = J_c$ for the F band. Since the T dependence of the magnon sideband intensity is determined by spin-correlation functions and is principally independent of the excited state of the single-exciton band (Ref. 35), it is difficult to explain the experimental result unless we assume the importance of some other effect connected with the symmetry of the excited state selecting the spin-exchange path along the a- or c-axis direction, which is involved in the correlation function.

[41]L. J. de Jongh and A. R. Miedema, Adv. Phys. 23, 1 (1974).

[42]G. G. Imbusch, in *Luminescence of Inorganic Solids*, edited by B. Di Bartolo (Plenum, New York, 1978), p. 155.

[43]W. W. Holloway, E. W. Prohofsky, and M. Kestigian, Phys. Rev. 139, A954 (1965).

[44]M. Morita and M. Kameyama, J. Lumin. 24/25, 79 (1981).

[45]F. J. Schäfer, W. Kleemann, and T. Tsuboi, J. Phys. C (in press).

[46]K. Namba and Y. Tanabe, J. Phys. Soc. Jpn. 37, 371 (1974).

[47]R. V. Pisarev, J. Ferré, R. H. Petit, B. B. Kirchertsov, and P. P. Syrnikov, J. Phys. C 7, 4143 (1974).